Soft Matter

COMMUNICATION

Cite this: *Soft Matter*, 2019, **15**, 5804

Received 13th April 2019,
Accepted 5th July 2019

DOI: 10.1039/c9sm00756c

rsc.li/soft-matter-journal

Microwave induced mechanical activation of hydrogel dimers†

Hamza K. Khattak, [a] Scott R. Waitukaitis [bc] and Aaron D. Slepkov *[a]

When grape-sized aqueous dimers are irradiated in a microwave oven, an intense electromagnetic hotspot forms at their point of contact, often igniting a plasma. Here we show that this irradiation can result in the injection of mechanical energy. By examining irradiated hydrogel dimers through high-speed imaging, we find that they repeatedly bounce off of each other while irradiated. We determine that an average of 1 μJ of mechanical energy is injected into the pair during each collision. Furthermore, a characteristic high-pitched audio signal is found to accompany each collision. We show that both the audio signal and the energy injection arise *via* an interplay between vaporization and elastic deformations in the region of contact, the so-called 'elastic Liedenfrost effect'. Our results establish a novel, non-contact method of injecting mechanical energy into soft matter systems, suggesting application in fields such as soft robotics.

The formation of plasma between a pair of grapes irradiated in a microwave oven has received considerable attention online[1,2] and in the recent literature.[3,4] The grapes act as a high-index aqueous dimer (or 'dumbell pair') whose geometry forms a localized electromagnetic hotspot at their point of contact.[3] This energy focusing is also possible with other aqueous materials such as sodium polyacrylate hydrogels—water saturated polymers that can contain more than 99% water by mass. In fields ranging from soft robotics[5–8] to microfluidics,[9,10] hydrogels are of particular interest for their elastic properties,[6,11,12] biocompatibility,[13] and diverse fabrication methods.[14,15] Activating these materials by injecting mechanical energy is often desireable, but pathways for achieving this are limited. Techniques such as pneumatics are common,[16–19] but typically require cumbersome tethering. Strategies for remote activation use chemical reactions,[20] swelling *via* hydraulics[7] or other means,[21] instabilities,[22] DC electric fields,[23] or heat-induced vaporization,[24–26] but only inject modest amounts of energy or require on-board power sources. Recent experiments have shown that bringing hydrogel spheres into contact with high-temperature (>100 °C) substrates leads to mechanical energy injection in the form of sustained bouncing.[24] This 'elastic Leidenfrost effect' arises from an interplay between vaporization and mechanical deformation, and provides robust energy injection at the cost of requiring proximity to a hot surface. In principle a similar effect could also occur during irradiation-induced vaporization, thus permitting rapid and fully remote activation, but so far this idea has not been explored.

We address this possibility experimentally by investigating the mechanical interaction of pairs of hydrogel spheres under microwave irradiation. The experimental setup is shown in Fig. 1A and B. We use a conventional microwave oven (1 kW, 2.45 GHz) to irradiate two 1.8 cm diameter hydrogel spheres. To keep the spheres together as an initially touching dimers, we set them on a gently curved parabolic track.‡ We observe their motion with a high-speed camera (MegaSpeed 55 K, 2000 fps at 1.3 MP) that images through a circular hole in the back of the oven (~20 pixel per mm resolution). Backlighting is provided by a 1 kW AC halogen lamp that illuminates the sample through the oven door, as shown in Fig. 1A. As the energy injection for hydrogels on hot surfaces is mediated by high-frequency (2–3 kHz) mechanical oscillations at the sphere–surface interface that produce audible sound,[24] we use a microphone to record audio during irradiation. The spheres are initially held apart at a distance of ~1 cm by a mechanical spacer. An experiment begins when this spacer is removed and the spheres are permitted to slide toward each other.

Examples of the phenomenon are shown in Fig. 1C and D. First, in panel C we show images of irradiated spheres taken with a color camera, which illustrates the clear formation of a plasma hotspot near the contact region (see Movie S1, ESI†). Second, in panel D we show black and white stills taken from

[a] *Department of Physics & Astronomy, Trent University, Peterborough, ON, Canada. E-mail: aaronslepkov@trentu.ca*
[b] *IST Austria, Am Campus 1, 3400, Klosterneuberg, Austria*
[c] *AMOLF, P.O. Box 41883 1009 DB, Amsterdam, The Netherlands*

† Electronic supplementary information (ESI) available: Supplementary text. Supplemental movies S1–S4. See DOI: 10.1039/c9sm00756c

‡ The profile of the track is approximated by $y = (7.4\ \mathrm{m}^{-1} \pm 0.3\ \mathrm{m}^{-1})x^2$.

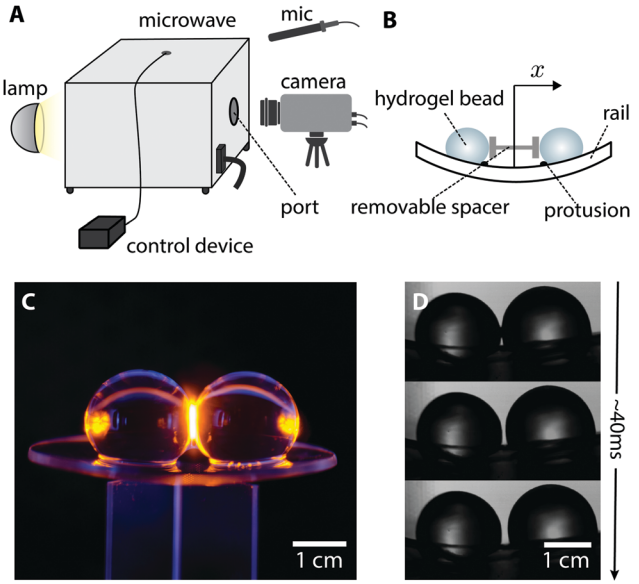

Fig. 1 (A) Experimental system. Hydrogel spheres inside a household microwave are imaged through a port in the back and back-lit through the front door. (B) Inside the oven, the spheres sit on a parabolic track (radius of curvature ~30 cm), which provides a well-defined restoring force to keep them in close proximity. Spheres are initially separated by a spacer, which is removed upon experiment initialization by a control device outside the oven. Two small protrusions on the track impart some angular velocity to each sphere to prolong their lifetime. (C) Illustrative photograph of plasma forming between a pair of hydrogel spheres during irradiation. The light on the outer edges of the spheres are refracted images of the plasma from the point of contact. See Movie S1 (ESI†) for video of the phenomenon. (D) Stills from high-speed video spanning ~40 ms, which demonstrate macroscale energy injection in the form of sustained bouncing (see Movie S2, ESI†).

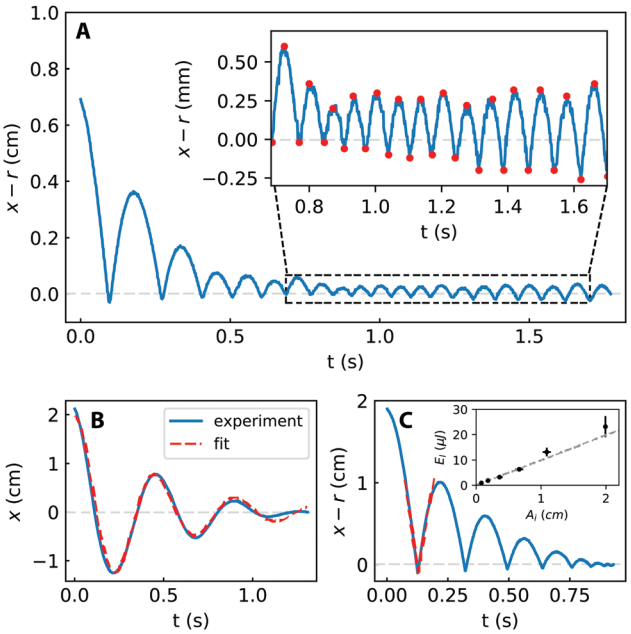

Fig. 2 (A) Center-of-mass position of a single sphere (minus its radius, r) as it bounces off its partner during microwave irradiation (see Movie S2, ESI†). Inset: Enlargement of the region of sustained bouncing, with maxima/minima indicated by red dots. (B) Example trajectory and fit to eqn (1) for a single sphere released with initial position of 2 cm. (C) Position of one sphere in a colliding pair without irradiation. The inset shows the energy lost in collisions *vs.* the preceding bounce amplitude A_i.

the high-speed video (see Movie S2, ESI†). These images are taken ~1 s after the spheres are released, which under normal circumstances would reveal stationary spheres with their mechanical energy already completely lost. However, as the images show, the spheres are in fact 'bouncing' off of each other with a maximum separation of ~1 mm. This mechanical activation continues for the duration of the experiment (3–4 s), which is limited only by the useful lifetime of the spheres.

We use images like the ones from Fig. 1D to track and plot the positions of each sphere (Fig. 2A). After the initial release, the spheres repeatedly bounce off of each other, visibly losing energy throughout the process. For times longer than ~1 s, this transient damps out entirely, leaving only steady-state microwave-induced bouncing. This is a clear indication that the spheres are converting electromagnetic energy into mechanical energy. The amount of energy injected per bounce can be calculated by noting that, for the approximately constant bounce amplitudes observed, the energy gained must be equal to the energy lost. We therefore consider the energy loss terms of our system in detail to quantify the injected mechanical energy.

First, we look at the dynamics of a single sphere, which involves gravitational potential energy (constrained by the parabolic track) and viscous damping losses during sliding. Importantly, rolling of the sphere is minimal due presence of a thin lubrication layer between the sphere and the track[27]—friction and subsequent friction-induced rolling are not significant.§ Releasing a sphere from a fixed position (Fig. 2B), we see that it exhibits underdamped oscillations before coming to rest. We model this system as a damped harmonic oscillator starting at rest with a solution of the form,

$$x(t) = x_0 e^{-\beta t}\left(\cos \omega t + \frac{\beta}{\omega}\sin \omega t\right). \quad (1)$$

Here, $x(t)$ is horizontal displacement, x_0 is the initial position, β is the viscous damping parameter, and ω is the oscillation frequency. Fitting this equation to the experimental results for a sample run (Fig. 2B), we extract values for β and ω. We use these parameters to determine the effective spring constant of the system, $k = (\omega^2 + \beta^2)m$, which characterizes the gravitational potential energy subject to the constraint of the curved surface,

$$U = \frac{1}{2}kx^2. \quad (2)$$

Performing experiments and fits for several runs, we find $k = (0.46 \pm 0.05)$ kg s^{-2} and $\beta = (2.3 \pm 0.3)$ s^{-1}. The value of k

§ Friction-induced rolling is negligible in our system, and in other hydrogel systems more generally.[27] We verify this with additional experiments, *e.g.*, Movie S4 (ESI†), where we observe nearly perfect sliding. This can be contrasted with similarly-sized friction-dominated materials (*e.g.*, grapes, also in Movie S4, ESI†), which exhibit nearly perfect rolling. We therefore do not consider rolling in our experimental analysis and subsequent model. For further discussion, see the ESI.†

is on par with what would be expected *via* the Lagrangian¶ [(0.43 ± 0.02) kg s^{-2}]. The agreement of the data with this model further verifies that losses at the sphere–surface interface are dominated by viscous effects in the lubrication layer. Using these parameters along with eqn (1) and the undamped energy relationship, $E = \frac{1}{2}kx^2 + \frac{1}{2}mv^2$, the energy loss due to damping can be calculated for a given trajectory.

Viscous damping during sliding is not the only source of energy loss. Owing to induced spheroidal vibrations and internal dissipation, collisions between the spheres also siphon energy. To measure these losses, we release two spheres without irradiation and focus on the effect of collisions on their speed (Fig. 2C), noting that

$$\Delta E_l = \frac{1}{2}m\left(v_{in}{}^2 - v_{out}{}^2\right), \quad (3)$$

where the speeds v_{in} and v_{out} can be measured using linear fits to the trajectories just before and after a collision (see ESI†). By plotting collisional energy loss against bounce amplitude (inset Fig. 2C), we find a simple linear relationship for the range of parameters relevant to our study.

Understanding the sources of energy loss, we are in a position to determine how much energy is injected during the steady bounce regime (Fig. 2A). We select a region of sustained bouncing (inset Fig. 2A) and measure an average bounce amplitude of (0.46 ± 0.01) mm and an average bounce period of (74 ± 5) ms. Using our previously determined damping parameter and the range of experimental bounce heights (0.5 ± 0.1) mm, we calculate the loss in energy for a sphere sliding twice the distance of the bounce amplitude, (0.22 ± 0.06) μJ. We add to this the collisional energy loss calculated from the linear fit in the inset to Fig. 2c, (0.48 ± 0.09) μJ. Despite significant variability from one bounce to the next, adding these energy losses allows us to determine an average energy injection (per sphere) of (0.6 ± 0.2) μJ.

For hydrogels exhibiting sustained bouncing on a hot surface, the energy injection is mediated by much smaller scale and higher frequency dynamics that occur during each collision. Owing to an interplay between vaporization and the elastic deformation of the soft hydrogel material, a small gap between the sphere and the hot surface repeatedly opens and closes at a frequency of a few thousand Hertz during each 'contact'.[24] Asymmetry in the pressure evolution during the opening and closing of the gap permits mechanical energy to be extracted from the expanding vapor, which both sustains the bouncing and leads to audible noise generation. We posit that similar microscale dynamics drive the energy injection in our system. Although working inside a microwave makes it difficult to image them directly, we find other evidence to support their existence. First, our high-speed videos reveal the presence of Rayleigh waves rippling away from the contact point [see Movie S2 (1 : 14), ESI†], which in the fixed hot-surface system are generated from the surface oscillations.[24] Second, thermal imaging of the dimer pair immediately after irradiation reveals a distinct hotspot at the point of contact, which can drive localized vaporization (Fig. 3A). Third, our microphone measurements reveal high-frequency acoustic pulses that temporally coincide with each collision event (Fig. 3B). Fig. 3C displays the power spectrum of these pulses averaged over several collisions, which highlights characteristic peaks between 2–3 kHz (see the ESI† for audio analysis methods). These are on par with the frequencies of the gap oscillations observed in the hot-surface system,[24] further suggesting a common mechanism.

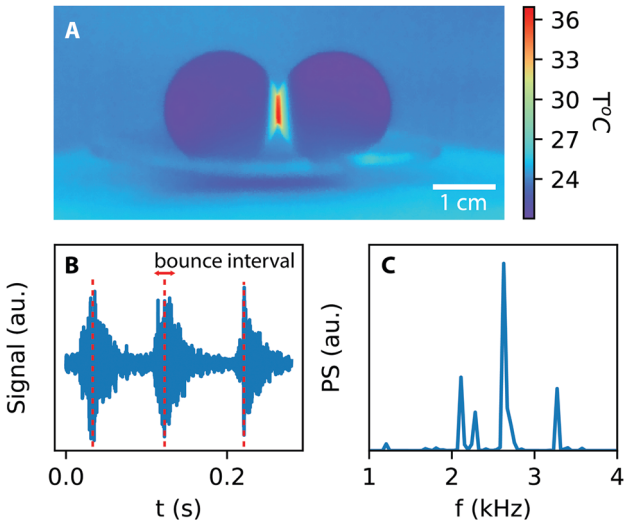

Fig. 3 (A) Thermal image of spheres after brief irradiation, which reveals intense localized heating at their point of contact. Note that this image is taken several seconds after irradiation has stopped; during irradiation we estimate that this hotspot quickly reaches 100 °C in the hydrogel and is much hotter in the surrounding vapor.[3] (B) Audio signals generated by a colliding dimer pair during irradiation. The dashed red lines indicate the timing of visually-confirmed collision events, which coincide with the noise generation. (C) The power spectrum of audio signals averaged over several collisions reveal distinct peaks between 2–3 kHz.

To understand the physics behind the energy injection, we consider the influence of heating from the electromagnetic hotspot in conjunction with the model of Waitukaitis[24] for the elastic Leidenfrost effect. This leads to the 5-stage cartoon outlined in Fig. 4A. First, initially separated spheres slide toward each other (stage i). When they touch, heating from the increasingly intense electromagnetic hotspot causes rapid vaporization in the region of contact (stage ii). Initially this vapor is trapped in a pocket between the spheres, which leads to a buildup of pressure. The growing pressure elastically deforms the spheres locally near the contact until a gap between them is opened (stage iii). Now the vapor escapes and the pressure rapidly diminishes, allowing the material in the contact region to elastically decompress (stage iv) and make contact again, thus initiating a new cycle (stage ii). These gap-pressure cycles continue throughout the entire collision, after which the spheres separate (stage v). Owing to the difference in the pressure evolution during the opening and closing of the gap, the cycles perform work on the spheres and inject a small

¶ To model $U = \frac{1}{2}kx^2$ we note $U = mgh$. If we fit a function $h = ax^2$ to the profile of the track, $k = 2mga$.

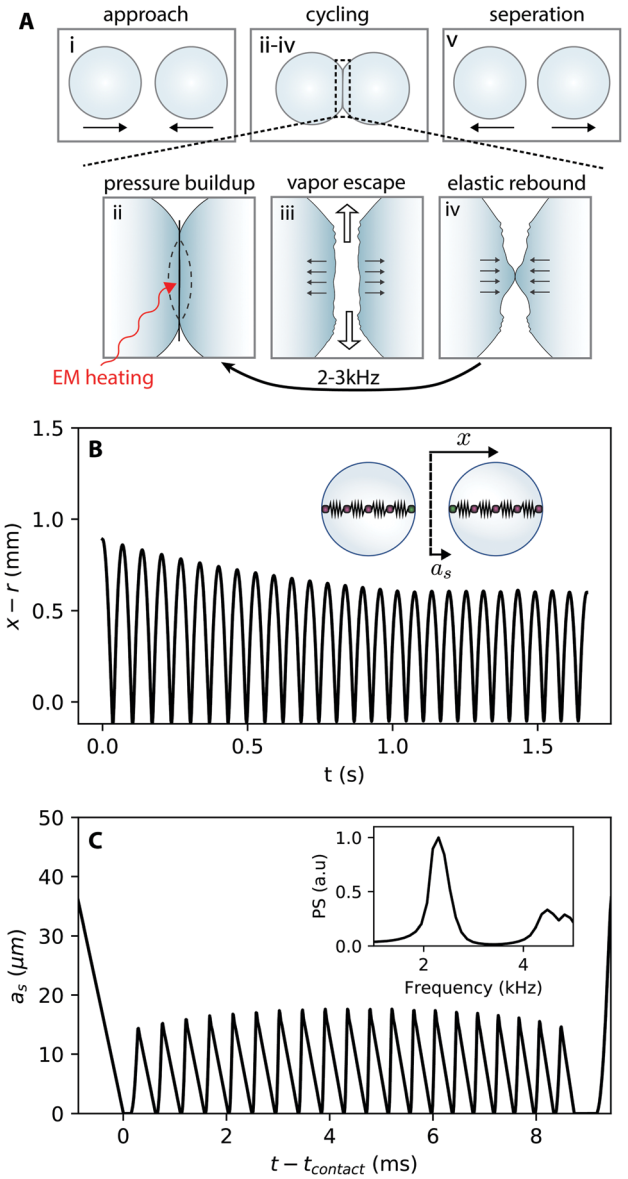

Fig. 4 (A) Diagram of the adapted energy injection mechanism.[24] In stage i spheres approach before a collision. In stage ii, pressure builds up in a pocket between the spheres due to microwave-induced electromagnetic heating and vaporization. The pressure grows until it opens a gap (stage iii), which allows vapor to escape. Once the pressure is sufficiently low, the surfaces elastically recoil (stage iv) and touch again, thus re-initiating stage ii. In stage *v* the spheres separate. (B) Position *vs.* time of a single sphere in a dimer pair as simulated by our model. Inset: Cartoon of mass-spring model used in simulations. (C) Simulated gap parameter, a_s, defined as half the distance between the innermost masses in the dimer pair, which illustrates the rapid opening and closing of a gap between them during a collision. Inset: Power spectrum of the gap oscillations in the main panel, which reveals peaks in the same 2–3 kHz band as our experimental audio data. See Movie S3 (ESI†) for videos of these simulated collisions as well as videos of undriven collisions.

amount of kinetic (and vibrational) energy relative to the non-irradiated case. In comparison to the bouncing of the spheres, which occurs on timescales of tens of milliseconds, these oscillations occur in just a few hundred microseconds and involve a compressional length scale that is orders of magnitude smaller. This separation of time and length scales means that the gap oscillations occur independently from the macroscopic bounce dynamics. The gross collisional features (*i.e.*, total duration and average compression force) are still governed by Hertzian contact dynamics, while the microscopic gap dynamics occur as a perturbation.

To implement this model, we carry out numerical simulations adapted from the approach of Waitukaitis *et al.*[24] Accounting for all aspects of the full time-dependent and three-dimensional multi-physics problem—which involves the electromagnetic supermode, the coupling of this to localized heating at the point of contact, the impact mechanics of the elastic spheres, the vaporization resultant from the localized heating, and the fluid dynamics of the escaping vapor—is beyond the scope of this work and would obscure the fundamental physics. We therefore simplify our numerics to include the essential ingredients at the cost of permitting only coarse comparison with our experimental results. The first simplification is to approximate each sphere as a chain of point masses connected by springs (inset Fig. 4A). Accounting for all forces in the system, we numerically integrate the equations of motion to capture the dynamics as these chains collide. This approach is appropriate not only because it allows one to simulate two colliding objects, but also because it permits resolution of the shorter length- and time-scales involved in the gap oscillations separately from the macroscopic (center-of-mass) dynamics. Each chain is attracted toward $x = 0$ with a potential given by eqn (2). We account for damping during sliding with a force proportional to each chain's center of mass velocity; collisional energy losses are inherently captured by excitation of each chain's internal vibration modes during collisions. We model the pressure buildup as occurring at a constant rate, α, when the gap between the spheres is closed. When the gap opens, we assume exponential decay with a time constant, τ. The masses and stiffness of the chains are calibrated from experiments, while the pressure evolution parameters (α and τ) are left free (see ESI† for further simulation details and Movie S3 for videos of simulated collisions). To track the microscale oscillations, we define a parameter, a_s, which is equal to half of the separation between the two bottom masses in the chain. The opening and closing of the gap is determined by a lengthscale l^*. When $2a_s < l^*$, the gap is considered closed. As in the experiments, we calculate macroscale energy injection (or energy loss in a 'non-irradiated' simulation) by considering the center-of-mass velocities before and after a collision.

In Fig. 4B, we plot the simulated trajectory of one sphere in a dimer pair. As can be seen, our numerical model indeed produces mechanical energy injection, allowing spheres to repeatedly bounce off of each other at a stable amplitude. The simulated bouncing frequency ($\sim$17 Hz) and amplitude ($\sim$0.6 mm) are close to the experimental observations ($\sim$14 Hz, 0.5 mm) shown in the inset of Fig. 2A. Furthermore, we recover the appropriate scale of energy injection (0.54 μJ for a single sphere) with the parameters $\alpha = 5$ GPa s^{-1}, $\tau = 2.5$ μs and $l^* = 25$ μm. These

correspond to an average vaporization rate ~ 1 mg per collision (see ESI† for calculation), which is comparable to the losses measured by Waitukaitis *et al.*[24] Focusing on the separation, a_s, between the edges of each chain during a single collison (Fig. 4C), we verify that our model produces gap oscillations between the two spheres when they are nominally in 'contact'. We determine the frequency of these oscillations by calculating the power spectrum (inset Fig. 4C), which reproduces the 2–3 kHz observed in our experiments. The agreement between our simple model and the experiments confirms that the elastic Leidenfrost mechanism is responsible for the energy injection during microwave irradiation of hydrogel dimers, but in this case the localized heating is triggered by the electromagnetic supermode.[3] While the process is mechanically seeded in this work by an initial separation of the spheres, this is primarily done to enable the reproducible measurement of injected mechanical energy upon irradiation. Hydrogel dimers in contact at rest are likewise activated to reach bouncing upon microwave irradiation. This is analogous to flash heating of a hotplate system and sets a lower bound on heating at the point of contact on the order of $\sim 100\ ^\circ\mathrm{C\ s^{-1}}$.[26] Since rotating spheres still vaporize at the point of contact, the true heating rate is likely higher, with local heating to $> 100\ ^\circ$C on the order of 100 ms.

The main aim of this study has been to report on a novel means of remote mechanical activation that arises when pairs of touching elastic aqueous spheres are irradiated with microwaves. The experimental conditions have been chosen for their balance of ease, repeatability, and optical access. Thus, none of the choices of hydrogel composition, mechanical loading, nor irradiation geometry have been optimized for maximal extraction of mechanical energy (bounce amplitude) or long-term hydrogel robustness. For example, commercially-obtained hydrogel spheres were hydrated to a specific size that is most likely to experience sparking, but is insufficiently mechanically strong to withstand long-term activation. Future progress, in particular for use in applications, will require fine-tuning of hydrogel stiffness and durability. Furthermore, while only quasi-horizontal loading has been shown, we anticipate the move to vertical axis loading and activation to be straightforward.

Conclusions

We have demonstrated that it is possible to inject mechanical energy into hydrogels by means of microwave irradiation. This manifests itself in the form of sustained bouncing between a pair of aqueous spheres, where in our system we measure ~ 1 μJ of injected energy during each collision in the steady state. Connecting our findings to the recently described elastic Leidenfrost effect,[24] whereby individual hydrogels siphon energy from a hot surface at a fixed temperature, we develop a distilled numerical model that recovers our key experimental results. Our findings present a new photonic energy delivery method for thermally activating mechanical motion in soft systems. The dynamic and untethered activation process could find novel applications in fields such as soft robotics, microfluidics, and active matter.

Funding

This work was supported by NSERC Discovery grant (RGPIN-2018-04491), the Canada Research Chairs program (#CRC-NSERC-231086), and the Netherlands Organization for Scientific Research (NWO-680-47-453).

Author contributions

ADS conceived the project. HKK and ADS designed the experiments. HKK built the apparatus and executed the experiments. HKK and SRW analyzed the results in consultation with ADS. HKK and SRW designed the simulations in consultation with ADS, and HKK carried them out. All authors contributed to the writing of the manuscript. SRW and ADS funded the research.

Conflicts of interest

There are no conflicts of interest to declare.

Acknowledgements

We thank Ontario Tech University for extended loan of a high speed camera. We thank undergraduate student Aaron Curtis for originally pointing out the ubiquity of irradiated dimer bouncing dynamics.

References

1 P. R. Michaud, *Fun with Grapes – A Case Study*, 1994, http://www.pmichaud.com/grape/.
2 D. Muller, *How Microwaving Grapes Makes Plasma*, 2019, https://youtu.be/wCrtk-pyP0I.
3 H. K. Khattak, P. Bianucci and A. D. Slepkov, *Proc. Natl. Acad. Sci. U. S. A.*, 2019, **116**, 4000–4005.
4 C. Bianchi, A. Datta and F. Dughiero, *Chem. Eng. Sci.*, 2019, **195**, 141–158.
5 J. Aguilar, T. Zhang, F. Qian, M. Kingsbury, B. McInroe, N. Mazouchova, C. Li, R. Maladen, C. Gong, M. Travers, R. L. Hatton, H. Choset, P. B. Umbanhowar and D. I. Goldman, *Rep. Prog. Phys.*, 2016, **79**, 110001.
6 H. Yuk, T. Zhang, S. Lin, G. A. Parada and X. Zhao, *Nat. Mater.*, 2016, **15**, 190–196.
7 H. Yuk, S. Lin, C. Ma, M. Takaffoli, N. X. Fang and X. Zhao, *Nat. Commun.*, 2017, **8**, 14230.
8 M. Ma, L. Guo, D. G. Anderson and R. Langer, *Science*, 2013, **339**, 186–189.
9 A. Sidorenko, T. Krupenkin, A. Taylor, P. Fratzl and J. Aizenberg, *Science*, 2007, **315**, 487–490.
10 D. J. Beebe, J. S. Moore, J. M. Bauer, Q. Yu, R. H. Liu, C. Devadoss and B. H. Jo, *Nature*, 2000, **404**, 588–590.

11 J. Y. Sun, X. Zhao, W. R. Illeperuma, O. Chaudhuri, K. H. Oh, D. J. Mooney, J. J. Vlassak and Z. Suo, *Nature*, 2012, **489**, 133–136.
12 J. N. Hunt, K. E. Feldman, N. A. Lynd, J. Deek, L. M. Campos, J. M. Spruell, B. M. Hernandez, E. J. Kramer and C. J. Hawker, *Adv. Mater.*, 2011, **23**, 2327–2331.
13 O. Jeon, K. H. Bouhadir, J. M. Mansour and E. Alsberg, *Biomaterials*, 2009, **30**, 2724–2734.
14 M. Workamp, S. Alaie and J. A. Dijksman, *Rev. Sci. Instrum.*, 2016, **87**, 125113.
15 S. Hong, D. Sycks, H. F. Chan, S. Lin, G. P. Lopez, F. Guilak, K. W. Leong and X. Zhao, *Adv. Mater.*, 2015, **27**, 4035–4040.
16 E. Brown, N. Rodenberg, J. Amend, A. Mozeika, E. Steltz, M. R. Zakin, H. Lipson and H. M. Jaeger, *Proc. Natl. Acad. Sci. U. S. A.*, 2010, **107**, 18809–18814.
17 R. F. Shepherd, F. Ilievski, W. Choi, S. A. Morin, A. A. Stokes, A. D. Mazzeo, X. Chen, M. Wang and G. M. Whitesides, *Proc. Natl. Acad. Sci. U. S. A.*, 2011, **108**, 20400–20403.
18 S. Sanan, P. S. Lynn and S. T. Griffith, *J. Mech. Robotics*, 2014, **6**, 31003.
19 B. Mosadegh, P. Polygerinos, C. Keplinger, S. Wennstedt, R. F. Shepherd, U. Gupta, J. Shim, K. Bertoldi, C. J. Walsh and G. M. Whitesides, *Adv. Funct. Mater.*, 2014, **24**, 2163–2170.
20 M. Wehner, R. L. Truby, D. J. Fitzgerald, B. Mosadegh, G. M. Whitesides, J. A. Lewis and R. J. Wood, *Nature*, 2016, **536**, 451–455.
21 T. Shen, M. G. Font, S. Jung, M. L. Gabriel, M. P. Stoykovich and F. J. Vernerey, *Sci. Rep.*, 2017, **7**, 16178.
22 H. Lee, C. Xia and N. X. Fang, *Soft Matter*, 2010, **6**, 4342–4345.
23 D. Morales, E. Palleau, M. D. Dickey and O. D. Velev, *Soft Matter*, 2014, **10**, 1337–1348.
24 S. R. Waitukaitis, A. Zuiderwijk, A. Souslov, C. Coulais and M. van Hecke, *Nat. Phys.*, 2017, **13**, 1095–1099.
25 S. Waitukaitis, K. Harth and M. Van Hecke, *Phys. Rev. Lett.*, 2018, **121**, 48001.
26 J. T. Pham, M. Paven, S. Wooh, T. Kajiya, H. J. Butt and D. Vollmer, *Nat. Commun.*, 2017, **8**, 905.
27 J. Kim and A. C. Dunn, *Soft Matter*, 2016, **12**, 6536–6546.